Accepted Manuscript

Synthesis, spectral characterization, thermal behavior, antibacterial activity and DFT calculation on N'-[*bis*(methylsulfanyl) methylene]-2-hydroxybenzohydrazide and N'-(4-methoxy benzoyl)-hydrazinecarbodithioic acid ethyl ester

M.K. Bharty, R.K. Dani, S.K. Kushawaha, Om Prakash, Ranjan K. Singh, V.K. Sharma, R.N. Kharwar, N.K. Singh

PII: S1386-1425(15)00219-X
DOI: http://dx.doi.org/10.1016/j.saa.2015.02.055
Reference: SAA 13357

To appear in: *Spectrochimica Acta Part A: Molecular and Biomolecular Spectroscopy*

Received Date: 21 October 2014
Revised Date: 15 February 2015
Accepted Date: 16 February 2015

Please cite this article as: M.K. Bharty, R.K. Dani, S.K. Kushawaha, O. Prakash, R.K. Singh, V.K. Sharma, R.N. Kharwar, N.K. Singh, Synthesis, spectral characterization, thermal behavior, antibacterial activity and DFT calculation on N'-[*bis*(methylsulfanyl) methylene]-2-hydroxybenzohydrazide and N'-(4-methoxy benzoyl)-hydrazinecarbodithioic acid ethyl ester, *Spectrochimica Acta Part A: Molecular and Biomolecular Spectroscopy* (2015), doi: http://dx.doi.org/10.1016/j.saa.2015.02.055

REVISED MANUSCRIPT

Synthesis, spectral characterization, thermal behavior, antibacterial activity and DFT calculation on N'-[*bis*(methylsulfanyl) methylene]-2-hydroxybenzohydrazide and N'-(4-methoxy benzoyl)-hydrazinecarbodithioic acid ethyl ester

M.K. Bharty[a*], R.K. Dani[a], S.K. Kushawaha[a], Om Prakash[b], Ranjan K. Singh[b], V. K. Sharma[c], R.N. Kharwar[c], N.K. Singh[a*]

[a]*Department of Chemistry,* [b]*Department of Physics,* [c]*Department of Botany, Banaras Hindu University, Varanasi, 221005, India.*

Abstract

Two new compounds N'-[*bis*(methylsulfanyl) methylene]-2-hydroxybenzohydrazide {Hbmshb (**1**)} and N'-(4-methoxy benzoyl)-hydrazinecarbodithioic acid ethyl ester {H_2mbhce (**2**)} have been synthesized and characterized with the aid of elemental analyses, IR, NMR and single crystal X-ray diffraction data. Compounds **1** and **2** crystallize in orthorhombic and monoclinic systems with space group P n a 21 and P21/n, respectively. Inter and intra molecular hydrogen bonding link two molecules and provide linear chain structure. In addition to this, compound **2** is stabilized by CH···π and NH···π interactions. Molecular geometry from X-ray analysis, geometry optimization, charge distribution, bond analysis, frontier molecular orbital (FMO) analysis and non-linear optical (NLO) effects have been performed using the density functional theory (DFT) with the B3LYP functional. The bioefficacy of compounds have been examined against the growth of bacteria to evaluate their anti-microbial potential. Compounds **1** and **2** are thermally stable and show NLO behavior better than the urea crystal.

Keywords: Crystal structure, Hydrogen bonding, Antibacterial property, Thermal stability, DFT calculation, NLO property.

*Corresponding author. Tel.: +91 542 6702447, E-mail: mkbharty@bhu.ac.in (M.K. Bharty), singhnk_bhu@yahoo.com (N.K. Singh).

1. Introduction

The chemistry of nitrogen-sulfur containing compounds is very interesting from the viewpoint of their electrical conductivity, molecular magnetism, electrochemical, biological and optoelectronic properties [1-5]. Metal complexes derived from N-aroyl hydrazinecarbodiothioic alkyl esters or dithiocarbazic acid esters have been studied [6-10] not only because of their intriguing coordination chemistry, but also because of their pronounced biological activities against microbes, viruses and cancer cells [11-13]. The potassium salt of N-(aroyl)-hydrazine carbodithioates are not very stable since they undergo intramolecular cyclization with elimination of H_2S forming 1,3,4-oxadiazole-2-thiones in the presence of acid or base [14] or on complexation [15, 16]. The main interest in the synthesis of esters is that they are much stable than the potassium salt and do not undergo cyclization to form oxadiazole derivatives. These S-alkyl/aryl hydrazine carbodithioic acid esters form complexes with a wide number of metal cations and show promising biological activity. A survey of literature shows that several papers are available on the syntheses and spectral characterization of substituted dithiocarbazates but there is very little work reported on the dithioester of N-acyl hydrazide, RC(O)NH-NH-C(S)SR which contain a similar -NH-C(=S) moiety as the S- alkyl esters of dithiocarbazic acid [11-13,17,18]. Following our interest in the synthesis and structural studies of compounds containing the H-N-C=S moiety responsible for biological activity, we report herein the preparation of N'-[*bis*(methylsulfanyl) methylene]-2-hydroxybenzohydrazide (Hbmshb) and N'-(4-methoxy benzoyl)-hydrazine carbodithioic acid ethyl ester (H_2mbhce) and their structural characterization, microbicidal properties and DFT calculation.

2. Experimental Section

2.1. Materials, Physical Measurements and method

Commercial reagents were used without further purification and all experiments were carried out in open atmosphere. Methyl salicylate and methyl 4-methoxybenzoate (Sigma Aldrich), CS_2 (S D Fine chemicals, India) and KOH (Qualigens) were used as received. Salicylic acid hydrazide was prepared by the reported method [19]. All the solvents were dried and distilled before use following the standard procedure. Carbon, hydrogen, nitrogen and sulfur contents were estimated on a CHN Model CE-440 Analyser and on an Elementar Vario EL III Carlo Erba 1108. IR spectra were recorded in the 4000–400 cm^{-1} region as KBr pellets on a Varian Excalibur 3100 FT-IR spectrophotometer. ^{1}H and ^{13}C NMR spectra were recorded in DMSO-d_6 on a JEOL AL300 FT NMR spectrometer using TMS as an internal reference. Five human bacterial pathogens *Salmonella typhi* (MTCC 3216), *Shigella flexneri* (ATCC 12022), *Staphylococcus aureus* (ATCC 25323), *Aeromonas hydrophila* (ATCC 7966) and *Enterococcus faecalis* were used to test the antibacterial activity of compounds **1** and **2**. Commercial antibacterial drugs, streptomycin sulphate and neomycin sulphate (Himedia) at the same concentrations (5-50 µg/disc) were used to compare effectiveness of the test compounds.

2.2. Synthesis

*2.2.1 Synthesis of N^2-[bis(methylsulfanyl) methylene]-2-hydroxybenzohydrazide (Hbmshb, **1**)*

Potassium N'-(2-hydroxy benzoyl)-hydrazine carbodithioate $[K^+(H_2L)^-]$ was prepared by adding CS_2 (1.5 mL, 20 mmol) dropwise to a suspension of salicylic acid hydrazide (3.042 g, 20 mmol) in methanol (30 mL) in the presence of potassium hydroxide (1.12 g, 20 mmol) and the reaction mixture was stirred continuously for 30 min. A white solid

[$K^+(H_2L)^-$] which separated was filtered, washed with EtOH and dried. Methyl iodide (1.2 mL, 20 mmol) was added dropwise to the methanol suspension of the above freshly prepared [$K^+(H_2L)^-$] (2.660 g, 10 mmol) and stirred continuously for 2 h at room temperature. The resulting yellow solution was concentrated and acidified with dilute CH_3COOH (20 % v/v) which yielded yellow precipitate of N^2-[*bis*(methylsulfanyl) methylene]-2-hydroxybenzohydrazide. This was filtered, washed with water and dried *in vacuo*. The precipitate was dissolved in methanol filtered and kept for crystallization which formed yellow crystals of compound **1**. Yield: 60 %. M.p. 185 ºC. Anal. Calc. for $C_{10}H_{12}O_2N_2S_2$ (256.36): C, 46.83; H, 4.68; N, 10.91; S, 24.98. Found: C, 46.84; H, 4.70; N, 10.86; S, 25.02 %. IR (cm^{-1}, KBr): ν(OH) 3301m, ν(NH) 3169m; ν(C=O) 1634s; ν(N–N) 1069; ν(C=S) 828. ^{1}H NMR (DMSO-d_6; δ ppm): 11.80 (s, 1H, OH), 9.70 (s, 1H, NH), 7.5-6.8 (m, 4H aromatic ring), 1.65 (s, 3H, -CH_3). ^{13}C NMR (DMSO-d_6; δ ppm): 203.12 (>C-S), 163.98 (>C=O), 158.97 (C1), 134.41 (C3), 128.58 (C5), 119.69 (C6), 117.32 (C4), 115.27 (C2), 16.85 (C9, C10).

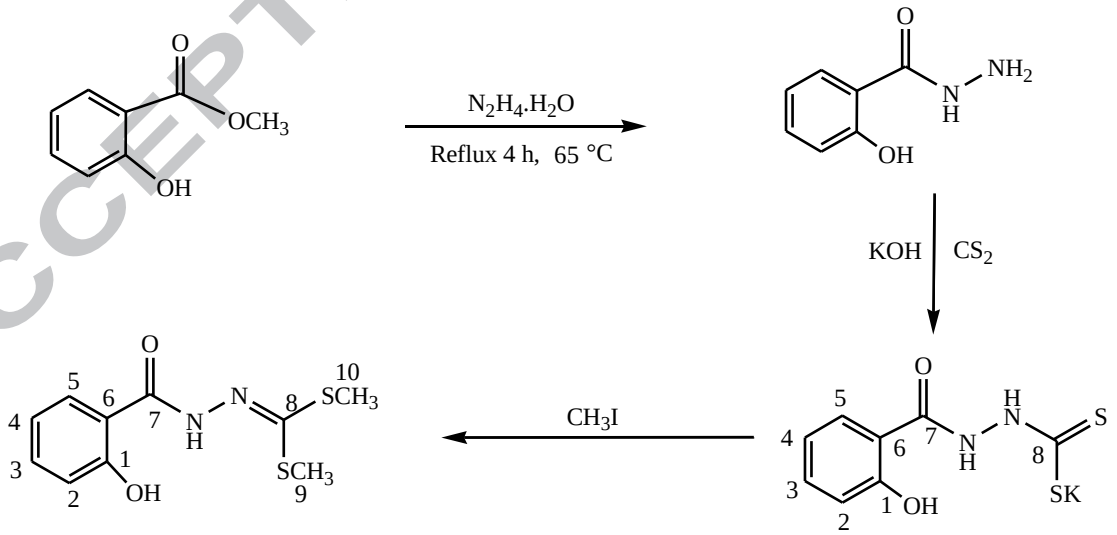

Scheme 1: Synthesis of N^2-[*bis*(methylsulfanyl) methylene]-2-hydroxybenzohydrazide

2.2.2. *Synthesis of N'-(4-methoxy benzoyl)-hydrazinecarbodithioic acid ethyl ester (H_2mbhce, **2**)*

$[K^+(H_2L')^-]$ was prepared as described above for the synthesis of potassium N'-(2-hydroxybenzoyl)-hydrazine carbodithioate $[K^+(H_2L)^-]$. N'-(4-methoxy benzoyl)-hydrazinecarbodithioic acid ethyl ester (H_2mbhce) was synthesized by adding ethyl iodide (1 mL, 10 mmol) dropwise to a methanol suspension of freshly prepared potassium [N'-(4-methoxy benzoyl) hydrazine] carbodithioate $[K^+(H_2L')^-]$ (2.804 g, 10 mmol) and stirring the reaction mixture for 2 h at room temperature. The resulting solution was filtered off and kept for crystallization which yielded colorless crystals of compound **2** suitable for X-ray analyses after 10 days. Yield: 50 %. M.p. 235 ºC. Anal. Calc. for $C_{11}H_{14}N_2S_2O_2$ (270.36): C, 48.82; H, 5.18; N, 10.36; S 23.67. Found: C, 48.90; H, 5.22; N, 10.35; S, 23.59 %. IR (ν, cm^{-1}, KBr): (NH) 3240m, (C=O) 1698s; (N-N) 1051; (C=S) 982. ^{1}H NMR (DMSO-d_6; δ ppm): 11.75, 11.43 (s, 2H, NH), 7.96-6.98 (m, 4H aromatic ring), 3.34 (-OCH_3), 2.58 (q, 2H). 2.47 (t, 3H). ^{13}C NMR (DMSO-d_6; δ ppm): 187.81 (C9=S), 163.85 (C8=O), 162.42 (C2-O), 128.41 (C6, C4), 125.05 (C5), 114.42 (C3, C7), 55.40 (-OCH_3), 39.26 (C10), 36.68 (C11).

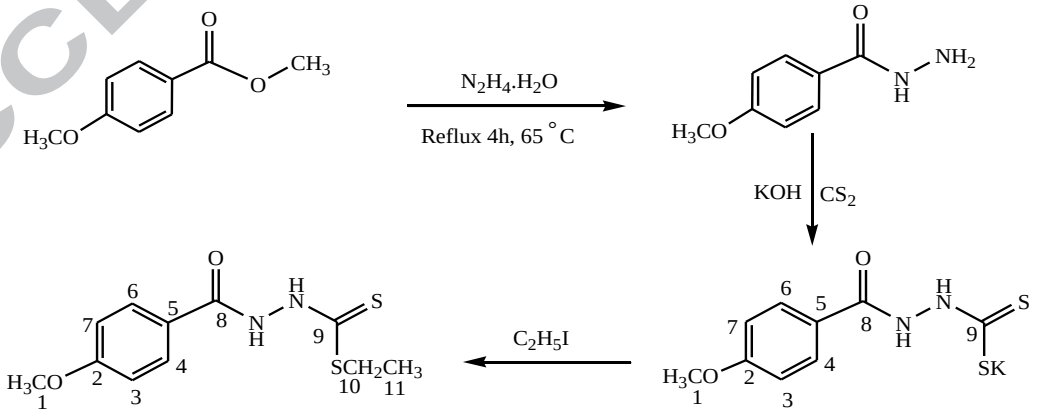

Scheme 2: Synthesis of N'-(4-methoxy benzoyl)-hydrazinecarbodithioic acid ethyl ester

3. Antibacterial assay

The antibacterial assay was done according to the reported method with slight modifications [20, 21]. The test compounds were dissolved in DMSO to a final concentration of 5mg/mL. Sterilized Whatman no. 1 filter paper discs (5 mm) were impregnated with different volume (1, 2, 4, 6, 8 and 10 µL) of compounds to get a final concentration of 5, 10, 20, 30, 40 and 50 µg per disc. Sterilized paper disc loaded with the 10 µL of DMSO was taken as a control. The bacterial test pathogens were spread on fresh Mueller Hinton Agar (MHA) plates with the help of cotton swabs to form an even lawn of the test bacteria. The filter paper disc impregnated with the test compounds were placed on the surface of the MHA plates seeded with test bacteria and the plates were incubated in a B. O. D. incubator (Caltan-152, Narang Scientific Works, New Delhi, India) for 24 h at 37±2 ºC. The inhibition zone around each disc was measured after 24 h of incubation. Inhibitory concentrations (IC_{50}) of compounds **1** and **2** were determined using broth dilution method by MTT (3-(4,5-dimethylthiazol-2-yl)-2,5-diphenyltetrazolium bromide) assay. The test compounds were dissolved in DMSO to a final concentration of 2 mg/ml. The test compounds were diluted to various concentrations (2, 4, 8, 16, 32, 64, 100 µg/mL) in 5 mL culture tube containing 2 mL Mueller-Hinton broth. One drop of exponentially growing culture of test bacterium was inoculated in each concentration of compounds and incubated at 37±2 ºC for 24 hours. A control was prepared using test bacterium and equal volume of the DMSO (100 µL) in Mueller-hinton broth without test compound. After incubation period, 200 µL MTT solution (5mg/ml) prepared in phosphate saline buffer (PBS) was added to each vial and incubated at 37±2 ºC for one hour. Culture was centrifuged at 10,000

rpm for 10 minutes and absorbance was observed at 570 nm. Minimum concentration of compounds which were able to inhibit 50 % activity of bacteria is considered as IC_{50}.

4. Crystal structure determination

Crystals suitable for X-ray analyses of the compounds were grown at room temperature. The crystal data were collected on an Oxford Gemini diffractometer equipped with a CrysAlis CCD software using a graphite mono-chromated Mo Kα (λ= 0.71073 Å) radiation source at 293 and 150 K for compounds **1** and **2,** respectively. Multi scan absorption correction was applied to the X-ray data collection for all the compounds. The structure was solved by direct methods (SHELXS-08) and refined against all data by full matrix least-square on F^2 using anisotropic displacement parameters for all non-hydrogen atoms. All hydrogen atoms were included in the refinement at geometrically ideal position and refined with a riding model [22]. The MERCURY package and ORTEP-3 for Windows program were used for generating structures [23, 24].

5. Results and discussion

Two new compounds N'-[*bis*(methylsulfanyl) methylene]-2-hydroxybenzohydrazide (**1**) and N'-(4-methoxy benzoyl)-hydrazinecarbodithioic acid ethyl ester (**2**) have been prepared by the reaction of methyl/ethyl iodide with potassium N-(aroyl) hydrazinecarbodithioate. The compounds are stable towards air and moisture and are soluble in methanol and ethanol from which they have been crystallized to get single crystals. Schemes 1 and 2 depict the formation of these compounds. The X-ray diffraction studies of compound **1** indicate that carbodithioate [-NHNHC(S)S^-] moiety has undergone thioenolization and the dithiol form reacted with methyl iodide to yield bis(methylsulfanyl) methylene group and both sulfur are

bonded with methyl group. In the case of compound **2**, only one ethyl group is attached to carbodithioate moiety without undergoing thioenolization.

5.1. IR spectra

The IR spectrum of N^2-[*bis*(methylsulfanyl) methylene]-2-hydroxy benzohydrazide (**1**) in KBr shows absorptions (cm^{-1}) due to the stretching modes of OH (3301), NH (3169), CH (2905), C=O (1634), N-N (1069) and C-S (828). The IR spectrum of N'-(4-methoxy benzoyl)-hydrazinecarbodithioic acid ethyl ester (**2**) shows absorptions (cm^{-1}) due to the stretching modes of NH (3240m), C=O (1698s), N-N (1051) and C=S (982) indicating the presence of –C(O)NH-NH-C(S)- group [25].

5.2. ^{1}H and ^{13}C NMR spectra

The ^{1}H NMR spectrum of Hbmshb (**1**) in DMSO-d_6 shows two signals at δ 11.80 and 9.70 ppm due the phenolic (OH) and hydrazinic (NH) protons, respectively. The aromatic protons appear as multiplet in the region of δ 7.5-6.8 ppm. The methyl protons are observed at 1.65 ppm. The ^{13}C NMR spectrum of Hbmshb shows signals at δ 203.12, 163.98, 158.97 ppm due to the C=S, C=O and C-O (phenolic) carbons, respectively. The phenyl ring carbons appear at δ 134.41 (C3), 128.58 (C5), 119.69 (C6), 117.32 (C4), 115.27 (C2) ppm while both methyl carbons are observed at δ 16.85 ppm. The ^{1}H NMR spectrum of H_2mbhce in DMSO-d_6 shows signals at δ 11.75, 11.43 and 3.34 ppm for the amide, thioamide and -OCH_3 protons, respectively. Four protons of the phenyl ring appear as multiplet in the range δ 7.96-6.98 ppm and methylene and methyl protons of ethyl group appear at δ 2.58 and 2.47 ppm, respectively. The ^{13}C NMR spectrum of H_2mbhce shows signals at δ 187.81, 163.85 and 162.42 ppm due to the C=S, C=O and C-O (methoxy phenyl) carbons, respectively. The methylene and methyl carbons appear at δ 39.26 and 36.68 ppm, respectively while other

methoxy phenyl carbons appear at δ 128.41 (C6, C4), 125.05 (C5), 114.42 (C3, C7) ppm. The methoxy -OCH_3 carbon is observed at δ 55.40 ppm.

5.3 Thermal behaviour

The thermal stability of compounds **1** and **2** were studied by TG and DTA in the temperature range 30-950 ºC under a nitrogen atmosphere by controlling heating rate of 10 ºC per minute using Perkin-Elmer simultaneous thermal analyzer (STA 6000). The thermograms (TG and DTA curves) reveal that the compounds are stable up to 180 ºC and indicate the absence of water molecule in crystalline phase [26]. Compounds **1** and **2** decompose in the temperature range 190-700 and 240-600 ºC, respectively (Fig. 1a) and the weight loss could be due to loss of organic moieties in the form of gaseous products through breaking of bonds. The later stage is slower and corresponds to the oxidation or vaporization of intermediate products in the temperature range 350-550 ºC indicating that thermolysis is exothermic in nature. Heating of samples above 700 ºC leaves no residue. The stability of these compounds are decided by the hydrogen bonding which is one of the most important non-covalent interactions and plays a vital role in building the supramolecular structures, making a great contribution to thermal stabilities. The presence of more intermolecular hydrogen bonding along with NH···π and CH···π interactions, compound **2** is more stable and this may be a probable reason that compound **1** decomposes earlier than compound **2**.

Compound **1** has a lower thermal stability due to low dimensionality since it melts between 184-196 ºC and absence of any thermal change before this temperature range indicates that sample restructuring does not take place before the degradation processes begins. Comparing the TG and DTA curves, it is observed that the major weight loss process starts after the melting temperature of the compounds. The DTA curve shows endothermic peak

(at 190 ºC) just after exothermic peak (at 180 ºC) in compound **1** which implies melting with slow decomposition, leading to volatilization upon heating further [27]. The DTA curve indicates that compound **2** undergoes an irreversible endothermic transition at 230 ºC, where melting begins and the endothermic peak represents the temperature at which the melting terminates at its melting point of 235 ºC. The sharpness of the peak in DTA curve of compound **1** indicates its good degree of crystallinity, purity and indicates that no phase transition occurs before melting. The DTA curves of compounds **1** and **2** show that after 350 and 450 ºC (Fig. 1b), respectively slow oxidation of the products takes place.

5.4. Antibacterial activity

Antibacterial activity of compounds **1**, **2** and commercial antibacterial drugs streptomycin sulphate and neomycin sulphate were tested against five human bacterial pathogens *Salmonella typhi* (MTCC 3216), *Shigella flexneri* (ATCC 12022), *Staphylococcus aureus* (ATCC 25323), *Aeromonas hydrophila* (ATCC 7966) and *Enterococcus faecalis*. A clear zone around the disc indicates the inhibitory activity of the compound on the organism. The results are given in Table 1 which indicates that the inhibitions by compounds are lower as compared to the standard drugs. The activity increases with increasing concentration of the compound and compound **2** is more active as compared to compound **1**. The highest zone of inhibition (2.3 cm) was recorded against *S. typhi* at 40 and 50µg/disc and minimum zone of inhibition was recorded in all cases at 5-20 µg/disc. Both the compounds are active against *E. faecalis* at all concentration range. It is clear that the zone of inhibition area is somewhat larger for compound **2** than **1**. The increased activity of compound **2** may be due to the presence of free HNCS moiety which is absent in compound **1** (Fig. 2a). Furthermore, free HNCS moiety increases the delocalization of π-electrons over the molecule of compound **2**

and enhances the lipophilicity which leads to the breakdown of the permeability barrier of the cell and thus retards the normal cell processes. The possible reason for the antibacterial action of compound **2** may be that it binds to the membranes of microorganisms through the hydrogen bonding with sulfur, prolonging the lag phase of the growth cycle and increasing the generation time of the organisms so that each organism takes more time to complete cell division. Although antibacterial activities of the compounds are lower as compared to the standard drugs streptomycin sulphate and neomycin sulphate but these compounds could be potentially used against weak bacterial pathogens.

Compound **2** is most effective against *Shigella flexneri* with IC_{50} value of 15.07 µg/mL followed by *Salmonella typhi* (30.64 µg/mL), *Enterococcus faecalis* (30.80 µg/ml), *Staphylococcus aureus* (37.23 µg/mL) and least effective against *Aeromonas hydrophila* (91.38 µg/ml). Similar trend (Table 2) is also observed for compound **1** with 32.38 µg/ml IC_{50} value for *Shigella flexneri*, 49.26 µg/mL for *Salmonella typhi*, 37.26 µg/mL for *Enterococcus faecalis*, 37.98 µg/mL for *Staphylococcus aureus* and 105.41 µg/ml for *Aeromonas hydrophila*. Fig. 2b shows that compound **2** is required in less amounts to inhibit the growth of bacteria as compared to compound **1**. Compound **2** shows impressively good activity against *Shigella flexneri* and *Salmonella typhi* with about 2.1 and 1.6 fold less IC_{50} values, respectively than compound **1**.

*5.5. Crystal structure description of compounds **1** and **2***

The molecular structures of compounds Hbmshb (**1**) and H_2mbhce (**2**) have been determined by single crystal X-ray diffraction data. The details of data collection, structure solution and refinement are listed in Table 3. Molecular structure diagrams for compounds **1** and **2** with atom numbering schemes are shown in Figs.3 and 4, respectively. Selected bond

lengths and angles are given in Tables 4 and 5. Weak intermolecular interactions are listed in Tables 6 and 7. In compound **2**, the C-S bond distances of 1.704(4) and 1.707(4) Å agree well with those in related compounds, being intermediate between 1.82 Å for a C-S single bond and 1.56 Å for a C=S double bond [28, 29] whereas for compound **1** the C-S bond distances of 1.758(9) and 1.774(14) Å indicate their single bond character. The distances and angles for Hbmshb (**1**) and H_2mbhce (**2**) are close to those reported earlier [30, 31]. In the solid state, compound **1** is stabilized *via* intermolecular C-H···O interaction between carbonyl oxygen and CH hydrogen atoms of aromatic ring and O-H···O interaction between hydroxyl hydrogen and carbonyl oxygen of a nearby molecule leading to the formation of linear chain (Fig. 5). The structure of compound **2** is stabilized *via* intermolecular N-H···O and C-H···O interactions occurring between carbonyl oxygen and hydrogen atoms of hydrazine (-NH), -OCH_3 and phenyl ring of a nearby molecule which leads to the formation of linear chains, whereas the C-H···S interaction between thione sulfur and hydrogen atoms of phenyl ring also contribute to the linear chain structure (Fig.6). The crystal structure of compound **2** is also stabilized *via* NH···π and CH···π interactions between the π electrons of phenyl ring and the hydrogens of hydrazine and methyl group, respectively.

5.6 Quantum chemical calculations

5.6.1. Optimization of geometry

All calculations and the geometry optimization for N^2-[*bis*(methylsulfanyl) methylene]-2-hydroxybenzohydrazide (**1**) and N'-(4-methoxy benzoyl)-hydrazine carbodithioic acid ethyl ester (**2**) have been performed with Gaussian 03 and Gauss View 4.1 [32] program packages using DFT method with functional B3LYP and basis set DFT/B3LYP/6-311G(d, p) [33, 34]. The input geometries for the DFT calculations were generated from single crystal X-ray

data. The optimized geometrical parameters are listed in Tables 4 and 5. The optimized geometries with charge distribution on atoms of molecules are shown in Fig. 7 and 8. The optimized energy for compounds **1** and **2** are -1444.819 and -1484.147 a.u. respectively which indicate that both compounds are stable. A slight disagreement in the bond lengths and angles are due to the fact that the experimental results have been collected for the solid phase and the theoretical calculations are done for the gas phase. In the solid state, the existence of crystal field along with the intermolecular interactions connect the molecules together, which results in the differences in bond parameters between the calculated and experimental values. The charges on the carbonyl oxygen of compounds **1** and **2** have almost comparable values whereas the charges on oxygen atoms of -OH and -OCH_3 are -0.412 and -0.338, respectively. On hydrazine moiety, the charge distributions on nitrogen are in the range -0.352 to -0.122 for compound **1** and -0.337 to 0.226 for compound **2**. Considering the method and basis set used in the atomic charge calculation, the oxygen and nitrogen atoms exhibit a negative charge which are donor atoms while the hydrogen atom exhibits a positive charge which is an acceptor atom for the formation of hydrogen bonding in the crystalline phase (Fig 7 and 12). The charge on the sulfanyl sulfur atom of compound **1** has a positive value, whereas the charge on the thioamide sulfur of compound **2** has a negative value (-0.176) which is responsible for N-H⋯S hydrogen bonding, whereas no such hydrogen bonding is observed in compound **1**.

5.6.2. Molecular electrostatic potential and Contour maps:

The molecular electrostatic potential (MEP) mapped surfaces illustrate the charge distributions of molecules three dimensionally which allow us to visualize variably charged regions of a molecule. The charge distributions of the molecules give clear signature of the

interactions of the molecules. The MEP mapped surface of the molecules are calculated by DFT/B3LYP/6-311G(d,p) method at the 0.02 isovalues and 0.004 density values. The molecular electrostatic potential (MEP) is a useful feature to study reactivity given that an approaching electrophile will be attracted to negative regions. In the majority of the MEP, the maximum negative region which is the preferred site for electrophilic attack are indicated as red color while the maximum positive region which is the preferred site for nucleophilic attack are symbolized in blue color. The importance of MEP lies in the fact that it simultaneously displays molecular size, shape as well as positive, negative and neutral electrostatic potential regions in terms of color grading. 3D plots of MEP for compounds **1** and **2** are shown in Figs. 9 and 10. The different values of the electrostatic potential at the surface are represented by different colors. Potential increases in the order red < orange < yellow < green < blue. The color code of these maps is in the range between -0.07931 to +0.07931 a.u. for compound **1** and -0.05576 to +0.05576 a.u. for compound **2** where blue indicates the strongest attraction and red, the strongest repulsion. Regions of negative V(r) are usually associated with the lone pair on electronegative atoms. As can be seen from the MEP map of compounds **1** and **2**, the regions having the negative potential are over the electronegative atom (oxygen/nitrogen) and the regions having the positive potential are over the hydrogen atoms. The green areas cover parts of the molecule where electrostatic potentials close to zero are the C-C, C-N and C-S bonds. The oxygen atoms have larger negative potential value than the nitrogen atoms. The positive regions are localized on the hydrogen atoms of CH_3 and C_2H_5 groups and on the ring. From this result, we can say that the hydrogen atoms indicate the strongest attraction and oxygen atoms indicate the strongest repulsion.

A contour map is a two-dimensional XY plot of a three-dimensional XYZ surface showing lines where the surface intersects planes of constant elevation (Z). The contour maps are also used to show lines of constant density or brightness, such as electrostatic potentials [35]. The contour maps are calculated by DFT/B3LYP/6-311G(d,p) method at the 0.02 isovalues and 0.004 density values at same level of calculations of the MEP mapped surface of the molecules. The electron rich red lines are around oxygen and nitrogen whereas electron deficient region are shown by greenish-yellow lines. Both have similar patterns of contour map as shown in Figs. 11 and 12.

5.6.3. Frontier molecular orbital (FMO) analysis

The HOMO energy characterizes the ability of electron transfer while the LUMO characterizes the ability of electron acceptance, and the gap between HOMO and LUMO characterizes the molecular chemical stability [36]. The HOMO-LUMO energy and the energy gap (ΔE) for the compounds have been calculated at DFT/B3LYP/6-311G(d,p) level and the results are given in Table 8. 3D plots of the HOMO and LUMO for compounds **1** and **2** are shown in Fig.13. It can be seen that the HOMO orbital is mainly located at the HNCS moiety of the compound as a result of the electron withdrawing effect of the OH and OCH_3 group, which in turn causes an increase in the LUMO electronic density as located on the aromatic ring. Methoxy phenyl and hydroxyl phenyl rings do not make any contribution to electron density of HOMO, whereas in LUMO the entire molecule contributes to form frontier molecular orbitals. The value of the energy separation between the HOMO and LUMO are 4.400627 and 4.575876 eV for compounds **1** and **2**, respectively. The small HOMO-LUMO energy gap means low excitation energy, a good stability and a low chemical hardness for the compound. The electronic transition from the ground state to the

excited state due to transfer of electrons from the HOMO to LUMO level is mainly a π···π transition. The chemical hardness of a molecule is defined by the formula [37]

$$\eta = \{-E_{HOMO} + E_{LUMO}\}/2$$

where E_{HOMO} and E_{LUMO} are the energies of the HOMO and LUMO molecular orbitals. The value of η for compounds **1** and **2** are 2.2003135 and 2.287938 eV, respectively which indicate that they are hard materials and compound **2** is harder than compound **1**. The above results indicate that compound **2** has better chemical activity and may effectively undergo intramolecular charge transfer upon excitation. The above results show that smaller the HOMO-LUMO energy gap, the larger the hyperpolarizability (see below) and compound **1** which has a substituted imine group (C=N double bond) may have potential applications in the development of NLO materials [38].

5.6.4. Global reactivity descriptors

The chemical reactivity and site selectivity of the molecular systems have been determined by the conceptual density functional theory [39]. Electronegativity (χ), chemical potential (μ), global hardness (η), global softness (S) and electrophilicity index (ω) are global reactivity descriptors and are highly successful in predicting global reactivity trends. On the basis of Koopman's theorem [36], global reactivity descriptors are calculated using the energies of

Frontier molecular orbitals E_{HOMO}, E_{LUMO} and given by Eqs. (a) – (e) [40-44].

$$\chi = -(E_{HOMO} + E_{LUMO})/2 = (I + A)/2 \quad \text{(a)}$$

$$\mu = -\chi = (E_{HOMO} + E_{LUMO})/2 = -(I + A)/2 \quad \text{(b)}$$

$$\eta = (-E_{HOMO} + E_{LUMO})/2 = (I - A)/2 \quad \text{(c)}$$

Where A and I are the ionization potential and electron affinity of the compounds respectively. Electron affinity refers to the capability of a ligand to accept precisely one electron from a donor. However, in many kinds of bonding *viz.* covalent hydrogen bonding, partial charge transfer takes place. Softness is a property of a compound that measures the extent of chemical reactivity and is the reciprocal of hardness.

$$S = 1/\eta \qquad \text{(d)}$$

Recently, Parr et al. [45] have defined a new descriptor to quantify the global electrophilic power of the compound as electrophilicity index (ω), which defines a quantitative classification of the global electrophilic nature of a compound. Parr et al. have proposed electrophilicity index (ω x) as a measure of energy lowering due to maximal electron flow between donor and acceptor. They have defined electrophilicity index (ω) as follows

$$\omega = \mu^2 \text{ S} = \mu^2/\eta \qquad \text{(e)}$$

This is positive and definite quantity and measures the stabilization in energy when the system acquires an additional electronic charge (ΔN) from the environment. The direction of the charge transfer is completely determined by the electronic chemical potential of the molecule because an electrophile is a chemical species capable of accepting electrons from the environments; its energy must decrease upon accepting electronic charge. Therefore its electronic chemical potential must be negative. When two molecules react, which one will act as an electrophile (nucleophile) will depend upon higher (lower) value of electrophilicity index. The high value of electrophilicity index shows that the compound is a strong electrophile. The usefulness of this new reactivity quantity has been recently demonstrated in understanding the toxicity of various pollutants in terms of their reactivity and site selectivity [46]. The calculated value of electrophilicity index describes the biological

activity for compounds. The energies of frontier molecular orbitals (E_{HOMO}, E_{LUMO}), energy band gap ($E_{HOMO} - E_{LUMO}$), electronegativity (χ), ionization potential *(A)*, electron affinity *(I)*, chemical potential (μ), global hardness (η), global softness (S) and global electrophilicity index (ω) for **1** and **2** are listed in Table 8.

5.6.5. Non-linear optical effect

Non-linear optical (NLO) effects arise from the interactions of electromagnetic fields in various media to produce new fields altered in phase, frequency, amplitude or other propagation characteristics from the incident fields [47]. NLO is at the forefront of current research because of its importance in providing the key functions of frequency shifting, optical modulation, optical switching, optical logic, and optical memory for the emerging technologies in areas such as telecommunications, signal processing, and optical interconnections [48, 49].

Second harmonic generation test was performed in order to find the NLO property of the grown crystal by using Kurtz-Perry technique [50]. Samples were prepared by crushing crystalline powder of compounds between two transparent glass plates and then exposed to picoseconds laser radiation at a wavelength of 1.907 μm. The second harmonic wave of 632 and 542 nm generated from the samples **1** and **2**, respectively was detected by photomultiplier tube after eliminating the pump light with a color filter and converted into electrical signal which was displayed on an oscilloscope and the signal amplitude in volts indicates the SHG efficiency of the samples. Urea crystals were used as the reference material and it was found that the SHG efficiency of compounds **1** and **2** are 8.3 and 7.1 times that of urea.

To support experimentally observed NLO property we have performed DFT calculation. The calculations of the mean linear polarizability (α_{tot}) and the mean first hyperpolarizability (β_{tot}) from the Gaussian output have been explained in detail previously [51], and DFT has been extensively used as an effective method to investigate the organic NLO materials [52]. The calculated total molecular dipole moment (μ_{tot}), linear polarizability (α_{tot}) and first-order hyperpolarizability (β_{tot}) are 5.0301 D, 25.469 $Å^3$ and 4.7653 x 10^{-30} cm^5/esu and 7.2718 D, 23.842 $Å^3$ and 3.942 x 10^{-30} cm^5/esu for compounds **1** and **2,** respectivily. Urea is one of the prototypical compounds used in the study of the NLO properties of molecular systems. Therefore it was used frequently as a threshold value for comparative purposes [37]. The values of μ_{tot}, α_{tot} and β_{tot} for urea are 3.53 D, 4.1446 $Å^3$ and 0.5883 X 10^{-30} cm^5/esu, obtained at the 6-311G (d,p). Theoretically, the first-order hyperpolarizability for compounds **1** and **2** are 8.1 and 6.7 times magnitude of urea. These results indicate that the compounds are good candidate as NLO material and may be used for application as non-linear optical material. Theoretical and experimental values are in agreement with each other.

The presence of various types of hydrogen bonding interaction in compounds makes the electron delocalization easier and decreases the value of the energy gap, as a result of which the absorption bands in the electronic spectrum may shift to the visible region and consequently, increases the nonlinear optical properties. The O-H···O and C-H···O interactions in compound **1** and N-H···O and C-H···O in compound **2** play an important role in making the structural unit, which enhances the overall electron transfer between donor and acceptor groups. The O-H···O hydrogen bond is known to have specific effects upon crystal packing and plays a very important role in NLO contributions to the total

nonlinearity [53]. The O-H···O hydrogen bond consists of two types of bonds: the shorter O–H bond and the longer H···O bond, which are dependent on each other. Due to the presence of above hydrogen bonding interaction, compound **1** shows more non linear optical effects than compound **2** and may be used as optoelectronic material. The presence of hydrogen bonds on optical nonlinearities of organic crystals has important implications in the structural design. Calculated and experimentally observed results show us, in the process of the material designing, that if we can optimize geometry of hydrogen bonds in crystals to the optimum space directions, excellent NLO crystals may be obtained and this gives us a useful clue that the crystal engineering should construct or optimize the space geometrical configures of hydrogen bonds with the optimum bond directions, and their potential NLO characteristics can be displayed up to the maximum.

6. Conclusion

This paper reports the syntheses, spectral, structural investigations and DFT calculations of N^2-[*b*is(methylsulfanyl) methylene]-2-hydroxybenzohydrazide (**1**) and N'-(4-methoxy benzoyl)-hydrazinecarbodithioic acid ethyl ester (**2**). In the solid state, both compounds are stabilized by various types of hydrogen bonding such as C-H···O, N-H···O and C-H···S. In addition, compound **2** involves CH···π and NH···π interactions. Antibacterial activity of compounds **1** and **2** were tested against five human bacterial pathogens which showed that the activity increases with concentration of the compounds. Compound **2** has better activity than compound **1** but lower than the standard drugs, streptomycin sulphate and neomycin sulphate. Compound **2** shows impressively good activity against *Shigella flexneri* and *Salmonella typhi* with about 2.1 and 1.6 fold less IC_{50} values respectively than compound **1**. The geometries of the compounds are optimized at B3LYP density functional theory level

which corroborate with the experimental data. The second harmonic generation (SHG) efficiency of the crystals was obtained by classical powder technique and it was found that the SHG efficiency of compounds **1** and **2** are 8.3 and 7.1 times that of urea. The NLO properties of the thermally stable compounds are much greater than that of urea which indicates that these compounds are good candidates as second-order NLO material. Due to the presence of O-H···O hydrogen bonding interaction, compound **1** shows more non linear optical effects than compound **2** and may be used as optoelectronic material.

7. Acknowledgement

One of the authors R.K. Dani thanks UGC, New Delhi for the award of RGNF (SRF). Dr. S.K. Kushawaha is thankful to the Department of Science and Technology, New Delhi, India for the award of a Young Scientist Project (No. SR/FT/CS-110/2011).

8. Supplementary material

CCDC 942774 and 960471 contain the supplementary crystallographic data for compounds. These data can be obtained free of charge from the Cambridge Crystallographic Data Center *via* www.ccdc.cam.ac.uk/data_request/cif.

References

[1] A.M. Bond, A.R. Hendrickson, R.L. Martin, J.E. Moir, D.R. Page, Inorg. Chem., 22 (1983) 3440-3446.

[2] N. Robertson, L. Cronin, Coord. Chem. Rev., 227 (2002) 93-127.

[3] M. Bousseau, L. Valade, J-P. Legros, P. Cassoux, M. Garbaukas, L.V. Interrante, J. Am. Chem. Soc., 108 (1986) 1908-1916.

[4] A.T. Coomber, D. Beljonne, R.H. Friend, J.L. Bredas, A. Charlton, N. Robertson, A.E., Underhill, Nature, 380 (1996) 144-146.

[5] N. Singh, A. Kumar, Synth. Met., 158 (2008) 442-446.

[6] M.A. Ali and M.T.H. Tarafder, J. Inorg. Nucl. Chem., 39 (1977) 1785-1791.

[7] M. Nazimuddin, M.A. Ali, F.E. Smith, M.A. Mridha, Transition Met. Chem.17 (1992) 74-78.

[8] M.A. Ali, M.H. Kabir, M. Nazimuddin, S.M.M.H. Majumder, M.T.H. Tarafder, M.A. Khair, Indian J. Chem. 27A (1988) 1064-1067.

[9] M.T.H. Tarafder, M.A. Ali, D.J. Wee, K. Azahari, S. Silong, D.A. Crouse, Transition Met. Chem. 25 (2000) 456-460.

[10] S. Gou, X. You, Z. Xu, Z. Zhou, K. Yu, Polyhedron 10 (1991) 1363-1366.

[11] M.A. Ali, C.M. Haroon, M. Nazimuddin, S.M.M.H. Majumder, M.T.H. Tarafder, M.A. Khair, Transition Met. Chem. 17 (1992) 133-136.

[12] M.E. Hossain, M.N. Alam, J. Begum, M.A. Ali, M. Nazimuddin, F.E. Smith, R.C. Hynes, Inorg. Chim. Acta 249 (1996) 207-213.

[13] M.E. Hossain, J. Begum, M.N. Alam, M. Nazimuddin, M.A. Ali, Transition Met. Chem. 18 (1993) 497-500.

[14] J.R. Reid, N.D. Heindel, J. Heterocycl. Chem. 13 (1976) 925-926.

[15] M.K. Bharty, A. Bharti, R.K. Dani, R. Dulare, P. Bharati, N.K. Singh, J. Mol. Struct. 1011 (2012) 34-41

[16] N.K. Singh, S.K. Kushawaha, M.K. Bharty, Ram Dulare, R.J. Butcher, J. Mol. Struct. 936 (2009) 257-263.

[17] A. Mitra, T. Banerjee, P. Roychowdhury, S. Chaudhuri, P. Bera, N. Saha, Polyhedron 16 (1997) 3735-3742.

[18] X.-H. Zhu, S.-H. Liu, Y.-J. Liu, J. Ma, C.-Y. Duan, X.-Z.You, Y.-P. Tian, F.-X. Xie, S.-S. Ni, Polyhedron 18 (1998) 181-185.

[19] N.K. Singh, A.K Pandey, M. Singh, M.K. Bharty, R. J. Butcher, Acta Cryst. Sec. E 63 (2007) 4327.

[20] A.W. Bauer, W.M. Kirby, J.C. Sherries, M. Turck Am J. Clin. Pathol, 45 (1966) 493-496.

[21] S. K. Gond, A. Mishra, V.K. Sharma, S.K. Verma, J. Kumar, R.N. Kharwar, A. Kumar, Mycoscience 53 (2012) 113-121.

[22] G.M. Sheldrick, Acta Cryst. A64 (2008) 112-122.

[23] I.J. Bruno, J.C. Cole, P.R. Edgington, M. Kessler, C.F. Macrae, P. McCabe, J. Pearson, R. Taylor, Acta Cryst. Sect. B58 (2002) 389-397.

[24] L.J. Farrugia, J. Appl. Cryst., 45 (2012) 849-854.

[25] N.K. Singh, M.K. Bharty, S.K. Kushawaha, U.P. Singh, Pooja Tyagi, Polyhedron 29 (2010) 1902-1909.

[26] A.H. Kianfar, L. Keramat, M. Dostani, M. Shamsipur, M. Roushani, F. Nikpour, Spectrochem. Acta A 77 (2010) 424-429.

[27] M. Arshada, Saeed-ur-Rehman, S.A. Khan, K. Masud, N. Arshad, A. Ghani, Thermochim. Acta 364 (2000) 143-153.

[28] T.S. Lobana, G. Bawa, A. Castineiras, R.J. Butcher, Inorg. Chem. Comm., 10 (2007) 506-509.

[29] T.S. Lobana, P. Kumari, R.J. Butcher, T. Akitsu, Y. Aritake, J. Perles, F.J. Fernandez, M.C. Vega, J. Organomet. Chem., 701 (2012) 17-26.

[30] J.P. Jasinski, R.J. Butcher, S.K. Kushawaha, M.K. Bharty, N.K. Singh, Acta Cryst. Sec. E 66 (2010) 1899.

[31] M.K. Bharty, A.K. Srivastava, R. Dulare, R.J. Butcher, N.K. Singh, Polyhedron 30 (2011) 990-996.

[32] M.J. Frisch, G.W. Trucks, H.B. Schlegel, G.E. Scuseria, M.A. Robb, J.R. Cheeseman, V.G. Zakrzewski, J.A. Montgomery, Jr.R.E. Stratmann, J.C. Burant, S. Dapprich, J.M. Millam, A.D. Daniels, K.N. Kudin, M.C. Strain, O. Farkas, J.B. V. Tomasi, M. Cossi, R. Cammi, B. Mennucci, C. Pomelli, C. Adamo, S. Clifford, J. Ochterski, G.A. Petersson, P.Y. Ayala, Q. Cui, D.K. Morokuma, A.D. Malick, K. Rabuck, J.B. Raghavachari, J. Foresman, J. Cioslowski, J.V. Ortiz, A.G. Baboul, B.B. Stefanov, G.L.A. Liu, P. Piskorz, I. Komaromi, R. Gomperts, R.L. Martin, D.J. Fox, T. Keith, M.A. Al-Laham, C.Y. Peng, A. Nanayakkara, M. Challacombe, P.M.W. Gill, B.Johnson, W. Chen, M.W. Wong, J.L. Andres, C. Gonzalez, M. Head-Gordon, E.S. Replogle, J.A. Pople, Gaussian 03, Revision A.1, Gaussian, Inc., Pittsburgh, 2003.

[33] A.D. Becke, J. Chem. Phys. 98 (1993) 5648-5652.

[34] C. Lee, W. Yang, R.G. Parr, Phys. Rev. B. 37 (1988) 785-789.

[35] R.K. Dani, M.K. Bharty, S.K. Kushawaha, Om Prakash, R. K. Singh, N.K. Singh, Polyhedron 65 (2013), 31-41.

[36] K. Fukui, Science 218 (1982) 747-754.

[37] G.A. Babu, P. Ramasamy, Curr.Appl.Phys. 10 (2010) 214-220.

[38] G. Tang, J. Zhaoa, Z. Jiang, S. Kou, X. Ju, C. Wei, Optics and Spectroscopy, 113 (2012) 240-258.

[39] R.G. Parr, W. Yang, Density Functional Theory of Atoms and Molecules, OxfordUniversity Press, Oxford, New York, 1989.

[40] R.G. Pearson, J. Org. Chem. 54 (1989) 1430-1432.

[41] R.G. Parr, R.G. Pearson, J. Am. Chem. Soc. 105 (1983) 7512–7516.

[42] P. Geerlings, F. De Proft, W. Langenaeker, Chem. Rev. 103 (2003) 1793–1873.

[43] R.G. Parr, L. Szentpály, S. Liu, J. Am. Chem. Soc. 121 (1999) 1922-1924.

[44] P.K. Chattaraj, U. Sarkar, D.R. Roy, Chem. Rev. 106 (2006) 2065-2091.

[45] J. Padmanabhan, R. Parthasarathi, V. Subramaniaan, P.K. Chattaraj, J. Phys.Chem. A 111 (2007) 1358-1361.

[46] R. John Xavier, P. Dinesh, Spectrochim. Acta A 113 (2013) 171-181.

[47] Y.-X. Sun, Q.-L. Hao, W.-X. Wei, Z.-X. Yu, L.-D. Lu, X. Wang, Y.-S. Wang, J. Mol. Struct. Theochem. 904 (2009) 74-82.

[48] V.M. Geskin, C. Lambert, J.-L. Bredas, J. Am. Chem. Soc. 125 (2003) 15651–15658.

[49] D. Sajan, H. Joe, V.S. Jayakumar, J. Zaleski, J. Mol. Struct. 785 (2006) 43-53.

[50] G.A. Babu, P. Ramasamy, Curr. Appl. Phys. 10 (2010) 214-220.

[51] Y.-X. Sun, Q.-L. Hao, Z.-X. Yu, W.-X. Wei, L.-D. Lu, X. Wang, Mol. Phys. 107 (2009) 223-235.

[52] S.K. Kurtz, T.T. Perry, J. Appl. Phys. 39 (1968) 3798-3813.

[53] D. Xue, S. Zhang, Chemical Physics Letters 301 (1999) 449-452.

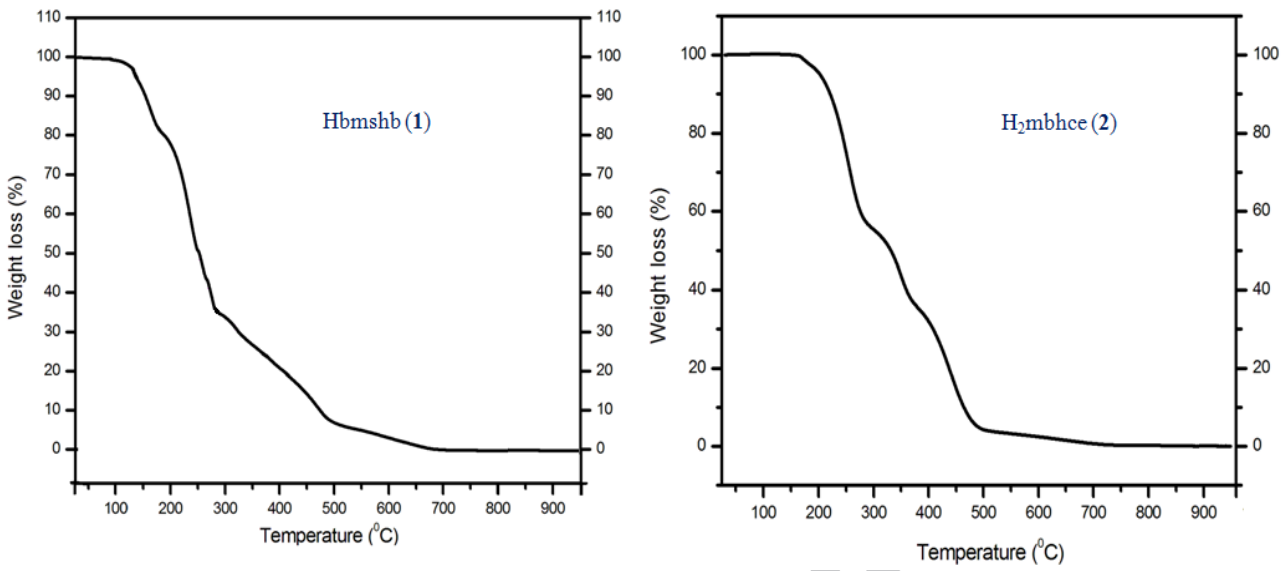

Fig.1(a) Thermograms of compounds **1** and **2**

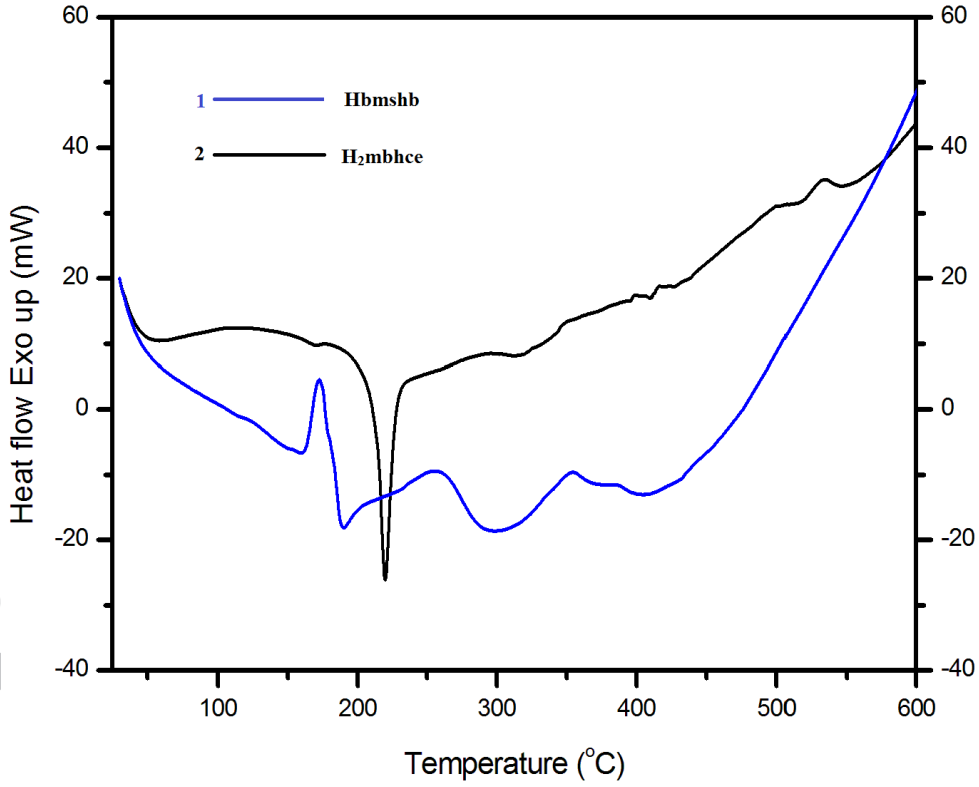

Fig.1(b) DTA curve of compounds **1** and **2**

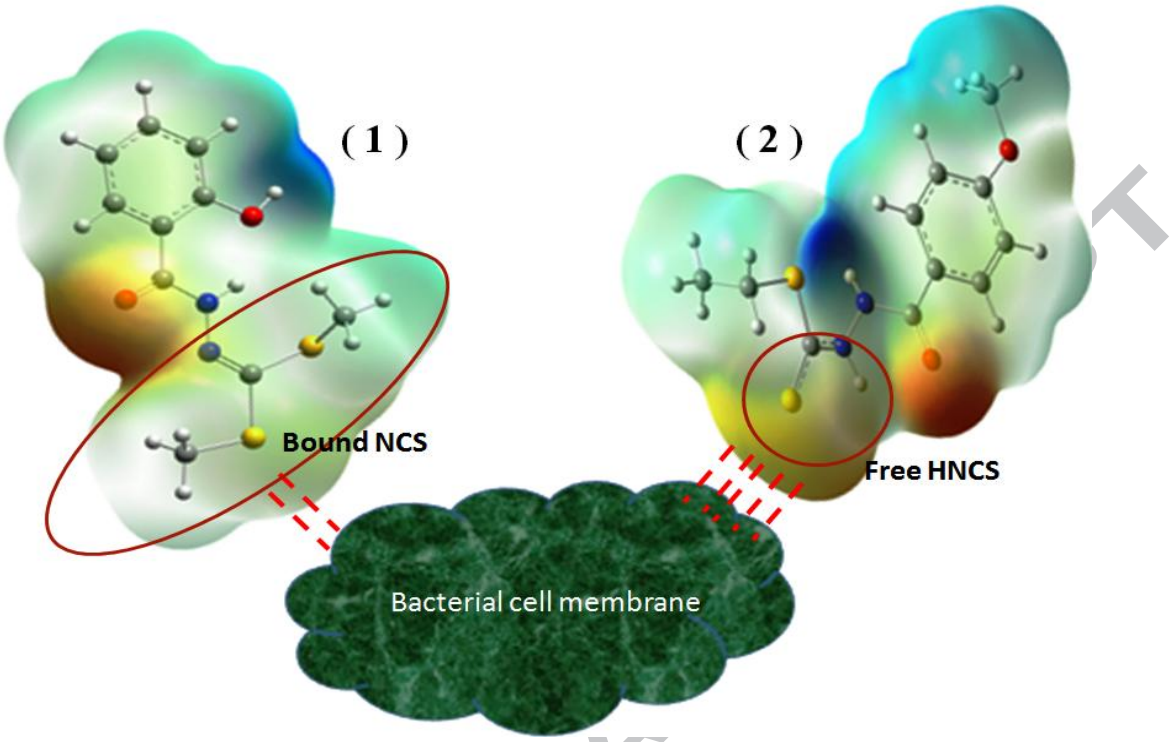

Fig.2(a) Mechanism of antibacterial activity for compounds **1** and **2**

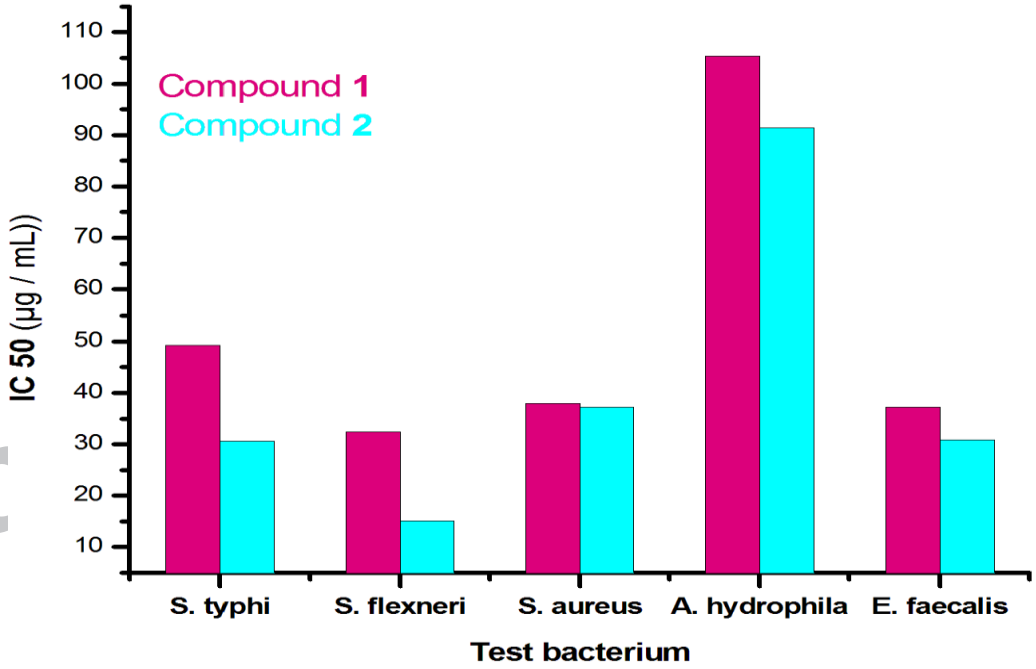

Fig.2 (b) Inhibitory concentration (IC_{50}) for compounds **1** and **2**

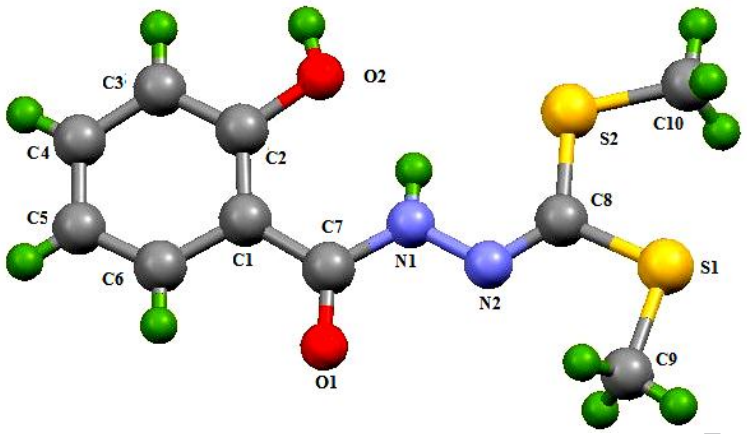

Fig.3. Molecular structure of N^2-[*bis*(methylsulfanyl) methylene]-2-hydroxybenzohydrazide (**1**)

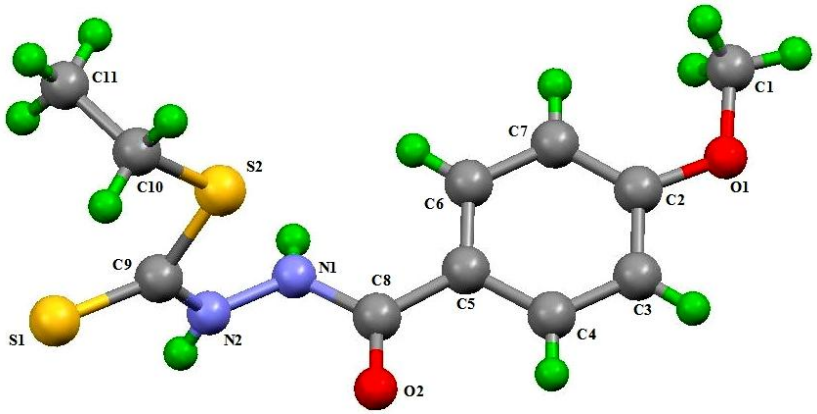

Fig.4. Molecular structure of N'-(4-methoxy benzoyl)-hydrazinecarbodithioic acid ethyl ester (**2**)

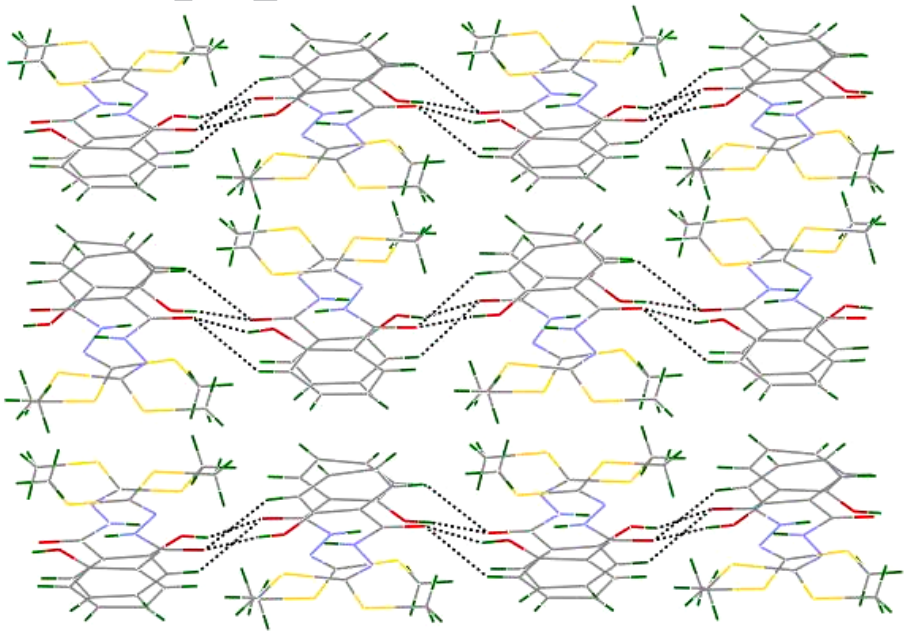

Fig.5. O-H···O and C-H···O interactions leading to linear structure in Hbmshb (**1**)

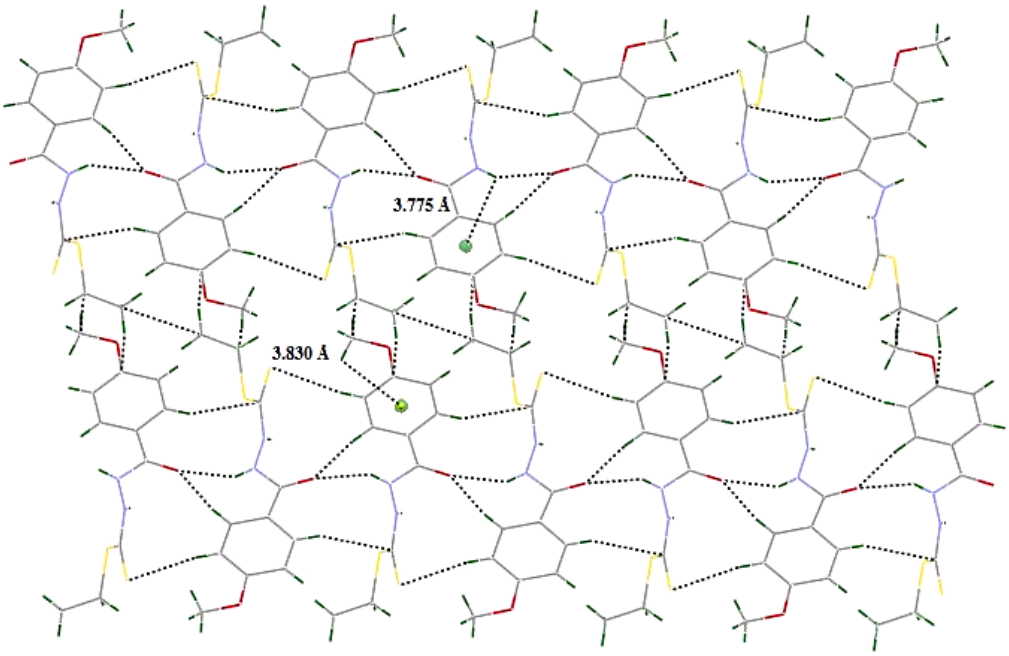

Fig.6. C-H···O, N-H···O and C-H···S hydrogen bonding and NH···π and CH···π interactions in H_2mbhce (**2**)

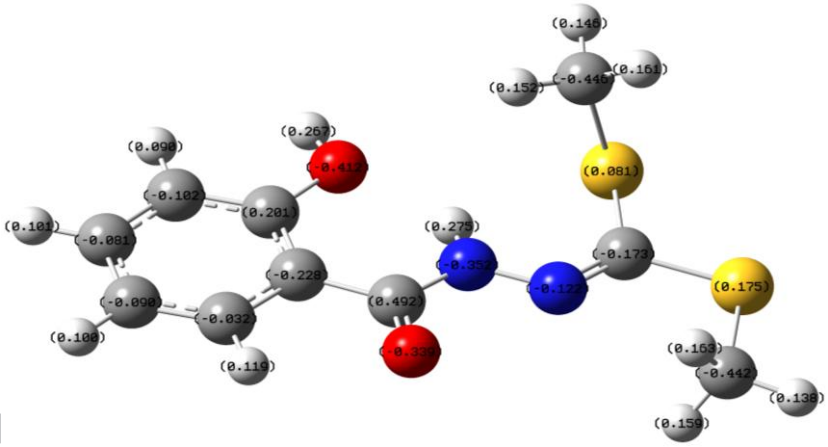

Fig.7. Optimize structure along with charge distribution on Hbmshb (**1**)

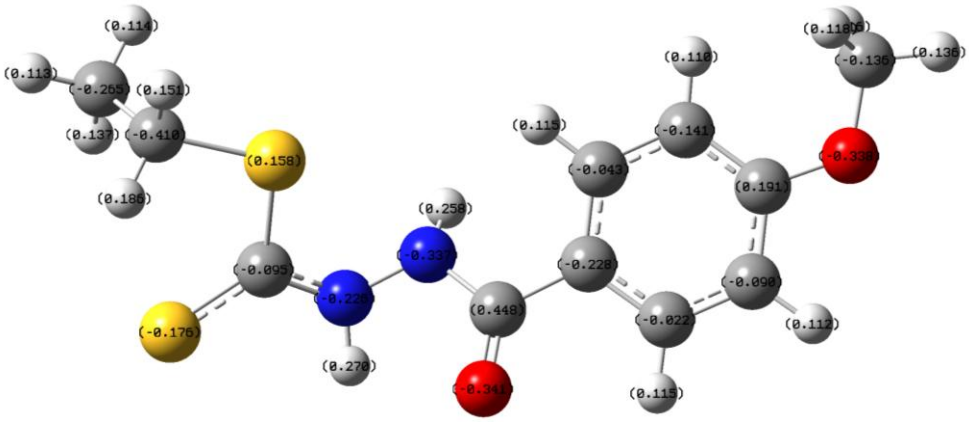

Fig.8. Optimise structure along with charge distribution on H_2mbhce (**2**)

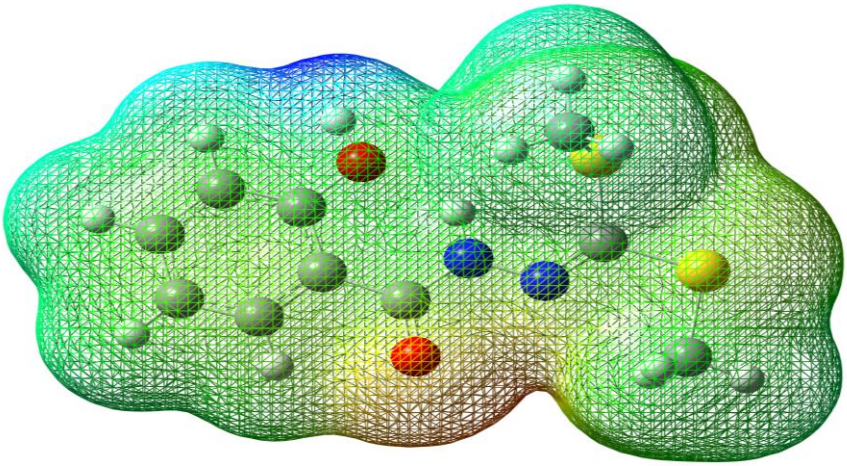

Fig.9. MEP plot of Hbmshb (**1**)

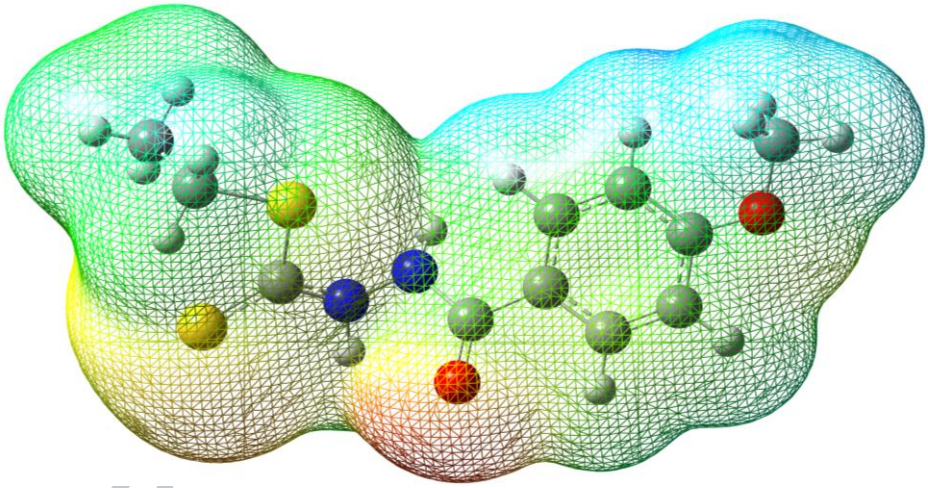

Fig.10. MEP plot of H_2mbhce (**2**)

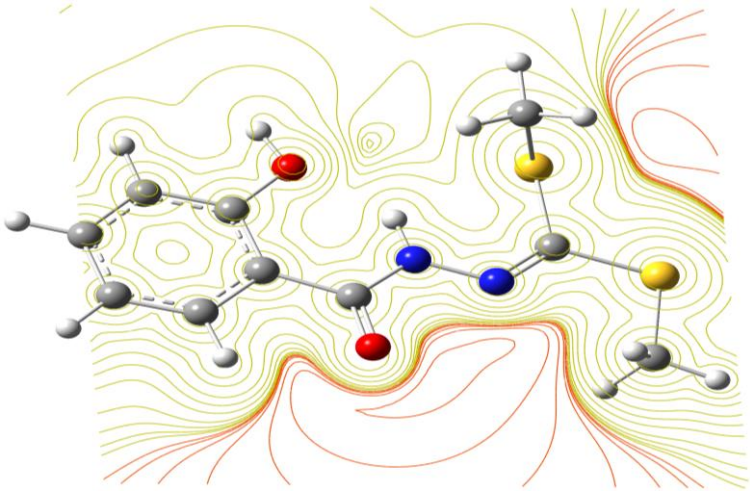

Fig.11. Contour map of Hbmshb (**1**)

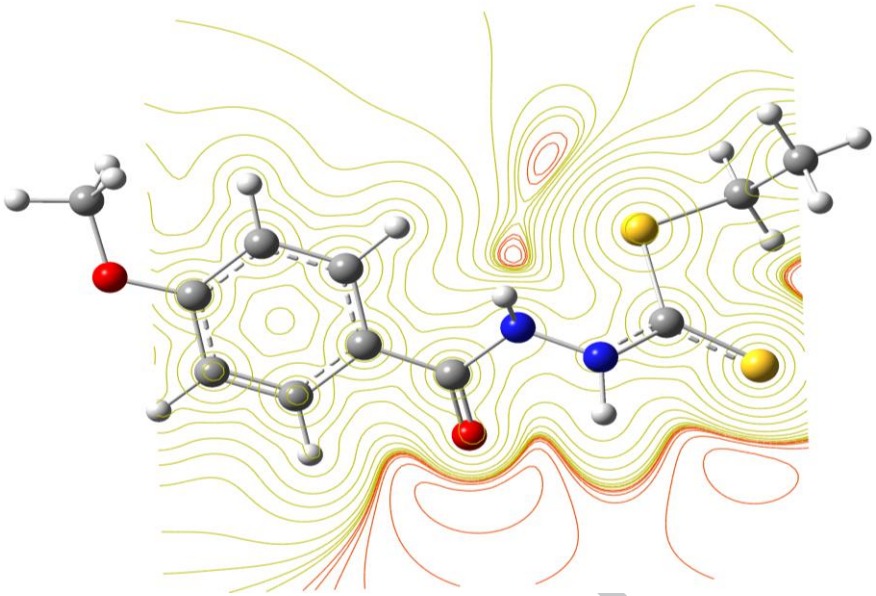

Fig.12. Contour map of H_2mbhce (**2**)

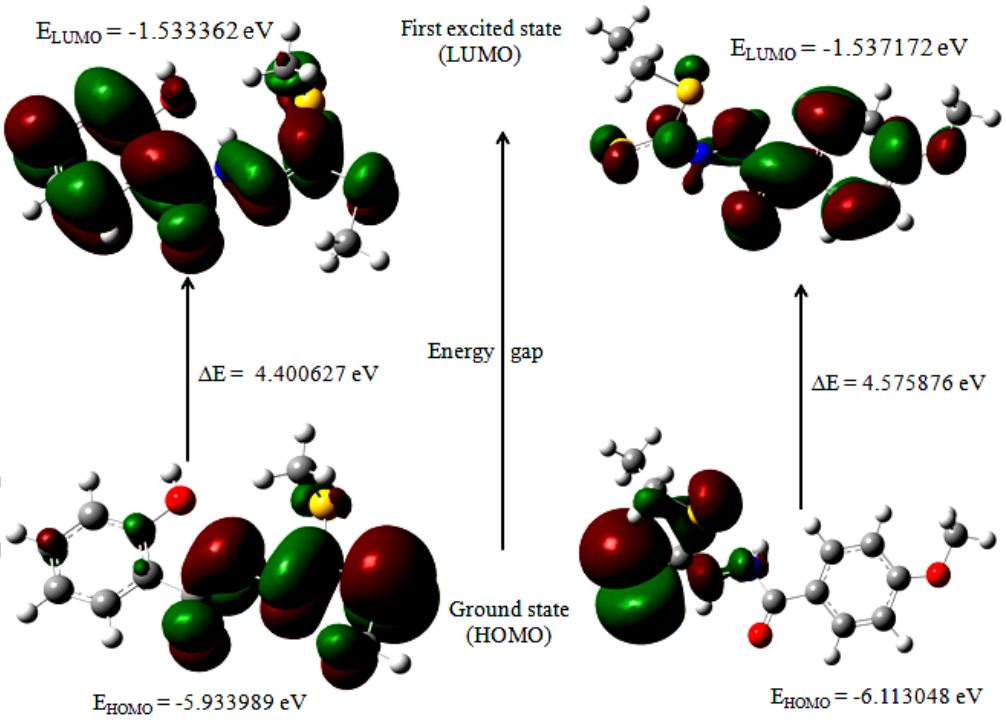

Compound **1** Compound **2**

Fig.13. Frontier molecular orbitals of molecule **1** and **2**

Table 1 Antibacterial assay of the compounds **1**, **2** and standard drugs against different human bacterial pathogens

Test pathogen	**Concentration of compound (µg/disc)**	**Compounds**		**Standard drug**		**Control (DMSO 10µl/ disc)**
		1	**2**	Streptomycin sulphate	Neomycin sulphate	
		Results of zone inhibition (cm)*				
Salmonella typhi (MTCC 3216)	5	-	0.8	2.4	1.8	-
	10	-	0.9	2.5	1.9	
	20	0.5	1.0	2.7	2.0	
	30	0.6	1.5	2.8	2.1	
	40	0.8	1.8	2.9	2.2	
	50	0.9	2.3	3.0	2.4	
Shigella flexneri (ATCC 12022)	5	0.7	-	0.8	1.5	-
	10	0.8	-	1.0	1.8	
	20	0.9	0.8	1.6	2.0	
	30	1.2	1.0	2.0	2.1	
	40	1.6	1.2	2.3	2.2	
	50	1.7	1.3	2.5	2.5	
Staphylococcus aureus (ATCC 25323)	5	-	-	1.8	1.75	-
	10	-	-	2.0	1.8	
	20	-	-	2.3	1.9	
	30	0.6	0.7	2.4	2.1	
	40	0.9	0.8	2.5	2.2	
	50	1.1	1.0	2.8	2.3	
Aeromonas hydrophila (ATCC 7966)	5	-	-	2.5	1.75	-
	10	0.5	-	2.6	2.0	
	20	0.7	0.6	2.7	2.15	
	30	0.8	0.7	2.8	2.3	
	40	0.9	0.8	2.9	2.4	
	50	0.9	0.9	3.0	2.6	
Enterococcus faecalis	5	0.5	0.7	1.9	1.8	-
	10	0.6	0.8	2.2	1.9	
	20	0.7	1.0	2.5	2.0	
	30	0.9	1.2	2.6	2.1	
	40	1.0	1.3	3.0	2.3	
	50	1.0	1.4	3.2	2.5	

- No zone was observed, *inhibition zone is the average of the diameter of zone from two sides in cm.

Table 2 IC_{50} of compounds **1** and **2** against different human bacterial pathogens.

Test bacterium	**IC_{50} (µg/mL)**	
	Compound **1**	Compound **2**
Salmonella typhi (MTCC 3216)	49.26	30.64
Shigella flexneri (ATCC 12022)	32.38	15.07
Staphylococcus aureus (ATCC 25323)	37.98	37.23
Aeromonas hydrophila (ATCC 7966)	105.41	91.38
Enterococcus faecalis	37.26	30.80

Table 3 Crystallographic data for the compounds **1** and **2**

Parameters	**1**	**2**
Formula weight	256.36	270.36
Crystal system	Orthorhombic	Monoclinic
Space group	P n a 21	P 21/n
T (K)	293(2)	150(2)
λ, Mo Kα (Å)	0.71073	0.71073
a (Å)	15.661(3)	6.3667(12)
b (Å)	12.829(17)	9.8412(18)
c (Å)	12.031(2)	20.783(3)
α (º)	90	90
β (º)	90	92.213(15)
γ (º)	90	90
V, ($Å^3$)	2417.2(7)	1301.2(4)
Z	8	4
ρ_{calcd} (g/cm^3)	1.409	1.380
μ (mm^{-1})	0.427	0.401
F(000)	1072	568
Crystal size (mm^3)	0.25 x 0.23 x 0.18	0.23 x 0.18 x 0.15
θ range for data collections (º)	3.05-29.20	3.18-32.58
Index ranges	$-21 \leq h \leq 21$ $-16 \leq k \leq 17$ $-16 \leq l \leq 16$	$-7 \leq h \leq 7$ $-11 \leq k \leq 11$ $-24 \leq l \leq 24$
No. of reflections collected	6937	9205
No. of independent reflections (R_{int})	4013	2285
No. of data/restrains/parameters	6554/0/2899	2285/0/164
Goodness-of-fit on F^2	1.234	0.981
R_1^a, wR_2^b [(I>2σ(I)]	0.0615, 0.1751	0.0645, 0.1624
R_1^a, wR_2^b (all data)	0.1086, 0.2122	0.0921, 0.1760
Largest difference in peak /hole ($e.Å^{-3}$)	1.368, -0.360	0.464, -0.461

$^a R_1 = \Sigma||F_o| - |Fc||\Sigma|F_o|.,$
$^b R_2 = [\Sigma w\,(|F^2_o| - |F^2_c|)^2/\Sigma w|F^2_o|^2]^{1/2}$

Table 4 Bond length (Å) and angles (°) for compound **1**

Bond length (Å)			Bond angles (°)		
	(Exp.)	(Cal.)		(Exp.)	(Cal.)
N1-N2	1.358(14)	1.356	C8- S1- C9	104.7(7)	102.3
N1-C7	1.364(14)	1.382	C8- S2- C10	101.6(6)	100.8
N2-C8	1.248(15)	1.275	N2 -C8 -S1	124.8(10)	126.5
S1-C8	1.758(9)	1.813	N2- C8 -S2	118.8(8)	120.6
S2-C8	1.774(14)	1.771	S1 -C8- S2	116.4(8)	113.1
S2-C10	1.779(12)	1.823	C8-N2-N1	115.8(10)	119.6
S1-C9	1.759(13)	1.839	N2- N1-C7	118.9(10)	119.4
C7-O1	1.215(13)	1.215	O1 -C7-N1	121.7(11)	122.4
C2-O2	1.381(13)	1.375	N1 -C7-C1	117.3(10)	116.2

Table 5 Bond length (Å) and angles (°) for compound **2**

Bond length (Å)			Bond angles (°)		
	(Exp.)	(Cal.)		(Exp.)	(Cal.)
O1-C1	1.435(5)	1.424	C9-S2-C10	99.4(2)	109.63
O1-C2	1.405(5)	1.355	C9-N2-N1	125.0(3)	121.93
O2-C8	1.239(4)	1.215	C3-C2-O1	115.5(4)	155.66
N1-C8	1.381(5)	1.401	O2-C8-N1	118.2(4)	120.75
N1-N2	1.424(5)	1.391	O2-C8-C5	123.2(3)	124.04
N2-C9	1.358(5)	1.364	N1-C8-C5	118.6(3)	115.19
S1-C9	1.704(4)	1.658	N2-C9-S1	124.2(3)	120.74
S2-C9	1.707(4)	1.782	N2-C9-S2	107.9(3)	112.33
S2-C10	1.827(5)	1.834	S1-C9-S2	127.9(3)	126.89

Table 6 Hydrogen bond parameters [Å and °] for compound **1**

Intermolecular hydrogen bonding				
D-H···A	d(D-H)	d(H···A)	d(D···A)	<(DHA)
C12-H12···O1	0.930	2.614	3.254	126.51
O4-H4A···O1	0.820	2.670	2.570	172.78
O2-H2···O3	0.830	1.813	3.279	158.86

Table 7 Hydrogen bond parameters [Å and °] for compound **2**

Intermolecular hydrogen bonding				
D-H···A	d(D-H)	d(H···A)	d(D···A)	<(DHA)
C7-H7···S1	0.950	2.027	3.717	141.33
C6H6···O2	0.950	2.675	3.568	157.02
N1-H1-O2	0.777	2.067	2.767	149.78

Table 8 Frontier molecular orbital energy for compounds **1** and **2**

Energy	**1**	**2**
Optimized energy E_{TOTAL} (a.u)	-1444.819186	-1484.147049
E_{HOMO} (eV)	-5.933989	-6.113048
E_{LUMO} (eV)	-1.533362	-1.537172
E_{LUMO}–E_{HOMO} (eV)	4.400627	4.575876
η (eV)	2.2003135	2.287938
I (eV)	5.933989	6.113048
A (eV)	1.533362	1.537172
χ (eV)	3.733675	3.871911
μ (eV)	-3.733675	-3.871911
S (eV)$^{-1}$	12.367047	11.823127
ω (eV)	6.337317	6.513592
Dipole moment (Debye)	5.0301	7.2718

Graphical Abstract (Synopsis)

Two new compounds N'-[*bis*(methylsulfanyl) methylene]-2-hydroxybenzohydrazide {Hbmshb (**1**)} and N'-(4-methoxy benzoyl)-hydrazinecarbodithioic acid ethyl ester {H_2mbhce (**2**)} have been synthesized. Inter and intra molecular hydrogen bonding link two molecules and provide linear chain structure. In addition to this, compound **2** is stabilized by CH···π and NH···π interactions. Molecular geometry from X-ray analysis, geometry optimization, charge distribution, bond analysis, frontier molecular orbital (FMO) analysis and non-linear optical (NLO) effects have been performed using the density functional theory (DFT) with the B3LYP functional. The bioefficacy of compounds have been examined against the growth of bacteria to evaluate their anti-microbial potential.

Graphical Abstract (Picture)

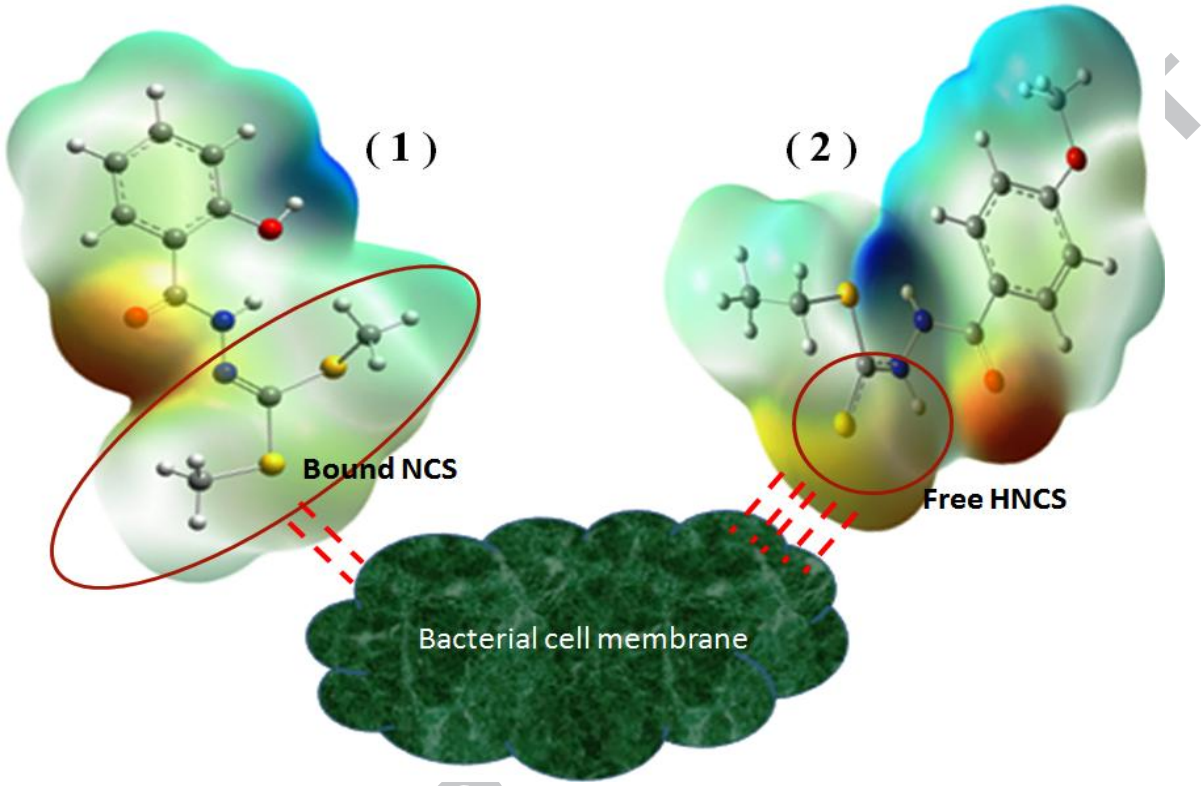

Research Highlights

- Two new N-aroyl-hydrazinecarbodithioic acid esters have been reported.
- Both compounds show NLO behavior better than the urea.
- Structural data from X-ray are corroborated well with DFT calculations.
- The compound **2** show antibacterial activity but lower than the standard drugs.
- These compounds may be potentially used against weak bacterial pathogens.